Electronic Supplementary Material (ESI) for Dalton Transactions.

Electron Supporting Information

For the Manuscript Entitled

Mononuclear complexes of amide-based ligands containing appended functional groups: Role of secondary coordination sphere on catalysis

Deepak Bansal,[a] Gulshan Kumar,[a] Geeta Hundal[b] and Rajeev Gupta*[a]

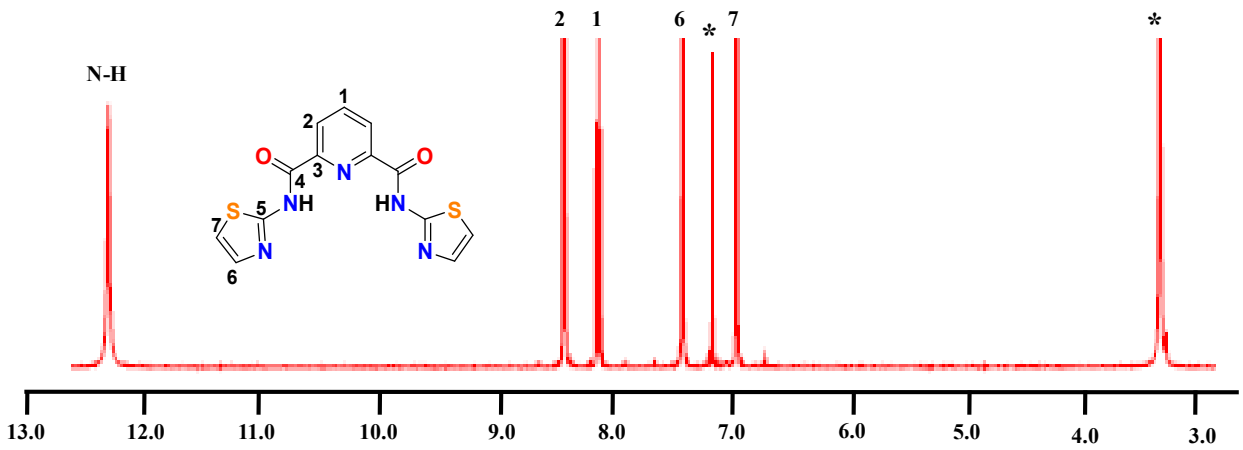

Figure S1. ^{1}H NMR spectrum of ligand H_2L^1 in $CDCl_3$. * Represents the residual solvent and/or adventitious H_2O.

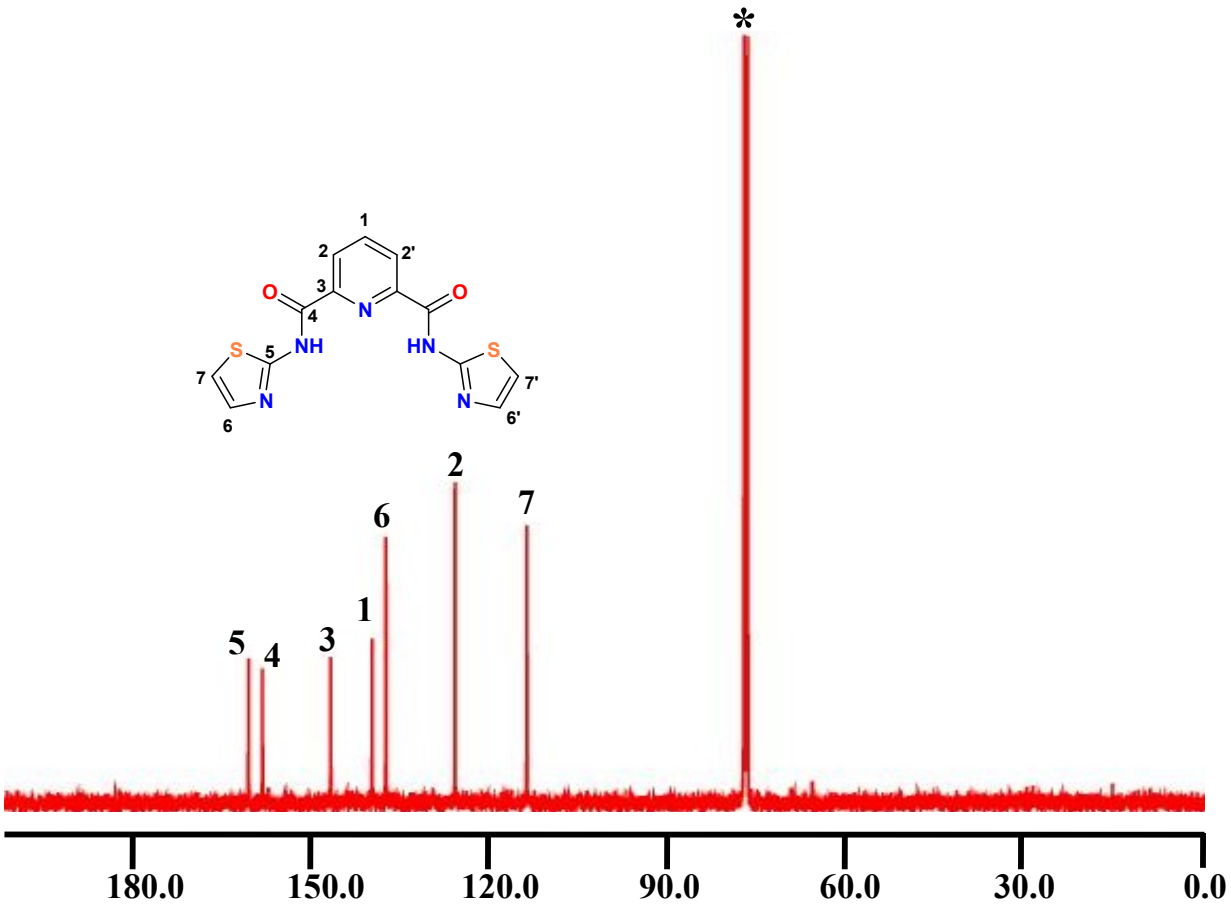

Figure S2. ^{13}C NMR spectrum of ligand H_2L^1 in $CDCl_3$. * Represents the residual solvent.

Figure S3. ^{1}H NMR spectrum of ligand H_2L^2 in $CDCl_3$. * Represents the residual solvent and/or adventitious H_2O.

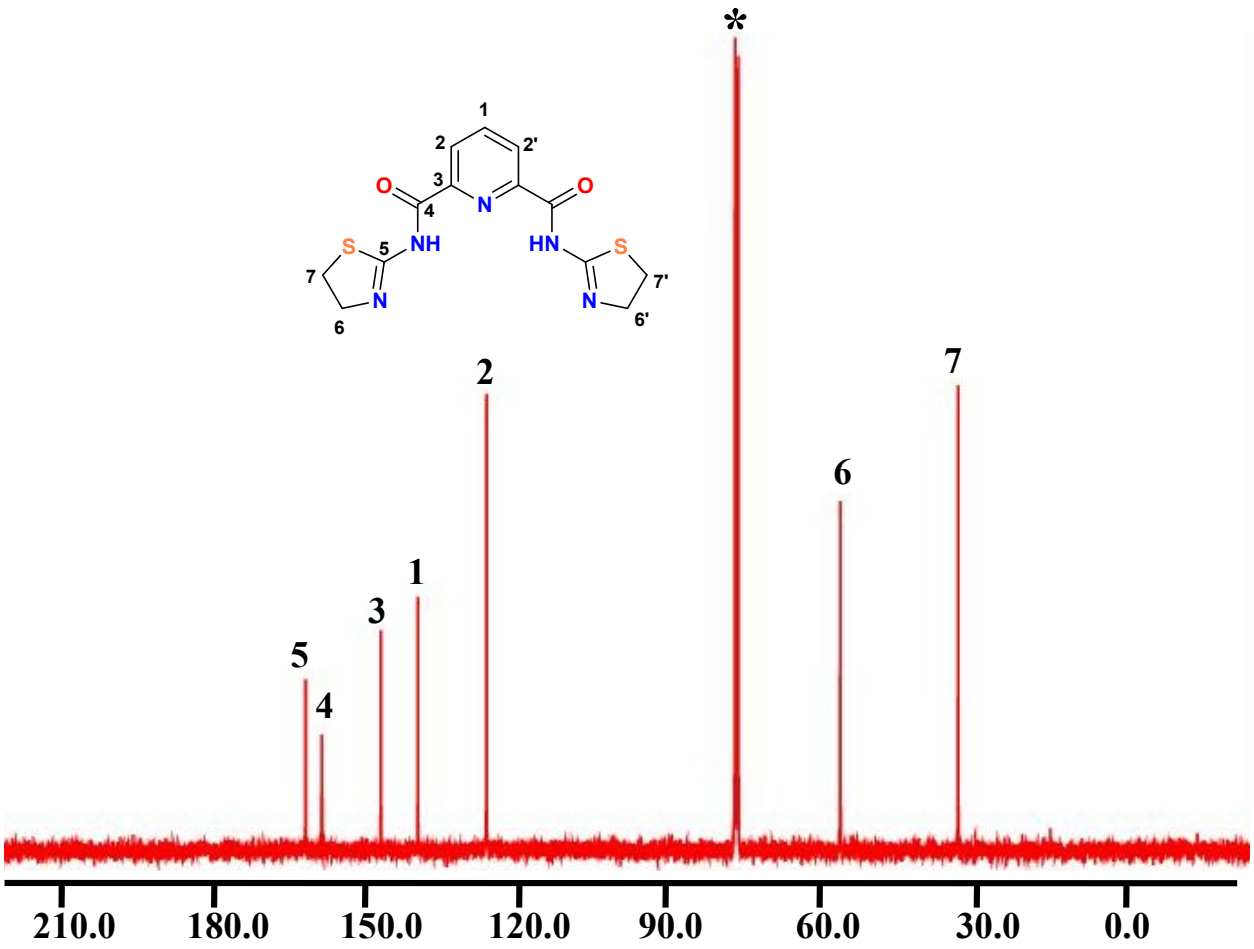

Figure S4. ^{13}C NMR spectrum of ligand H_2L^2 in $CDCl_3$. * Represents the residual solvent.

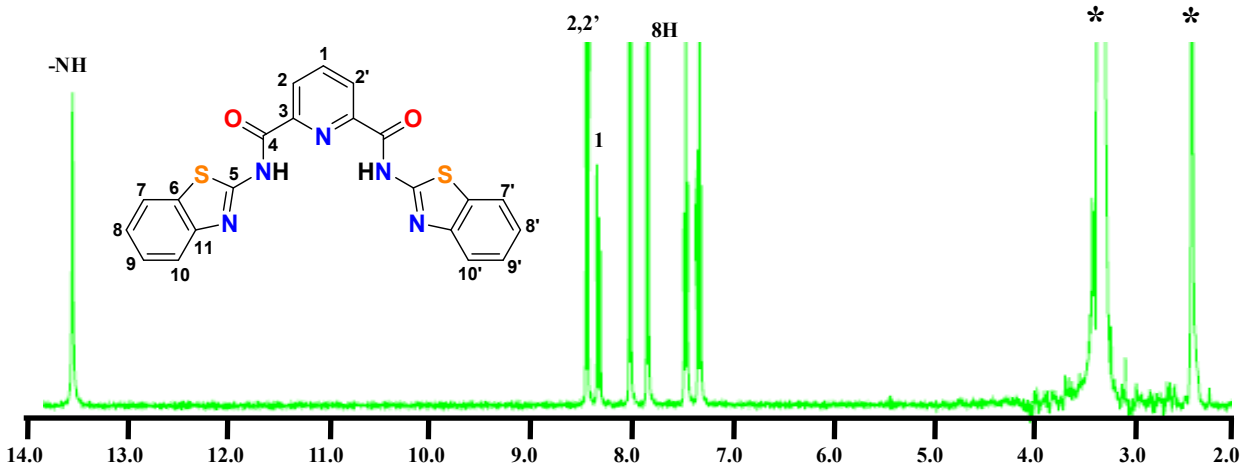

Figure S5. ^{1}H NMR spectrum of ligand H_2L^3 in D_6-DMSO. * Represents the residual solvent and/or adventitious H_2O.

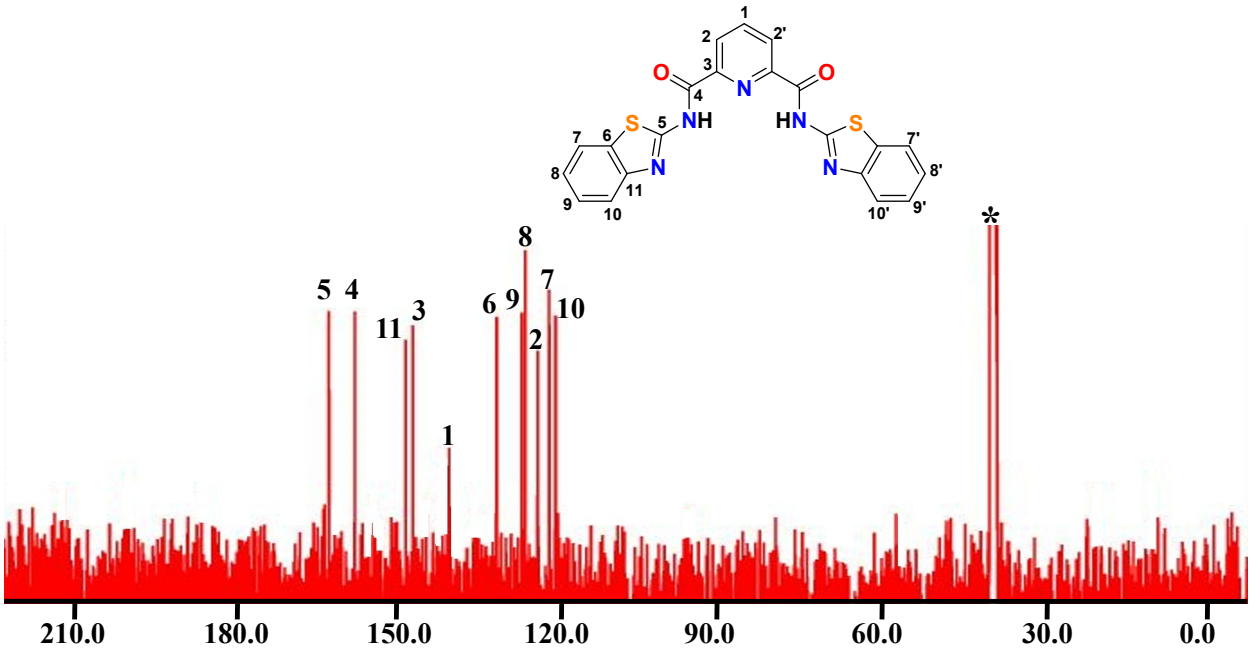

Figure S6. ^{13}C NMR spectrum of ligand H_2L^3 in d_6-DMSO. * Represents the residual solvent.

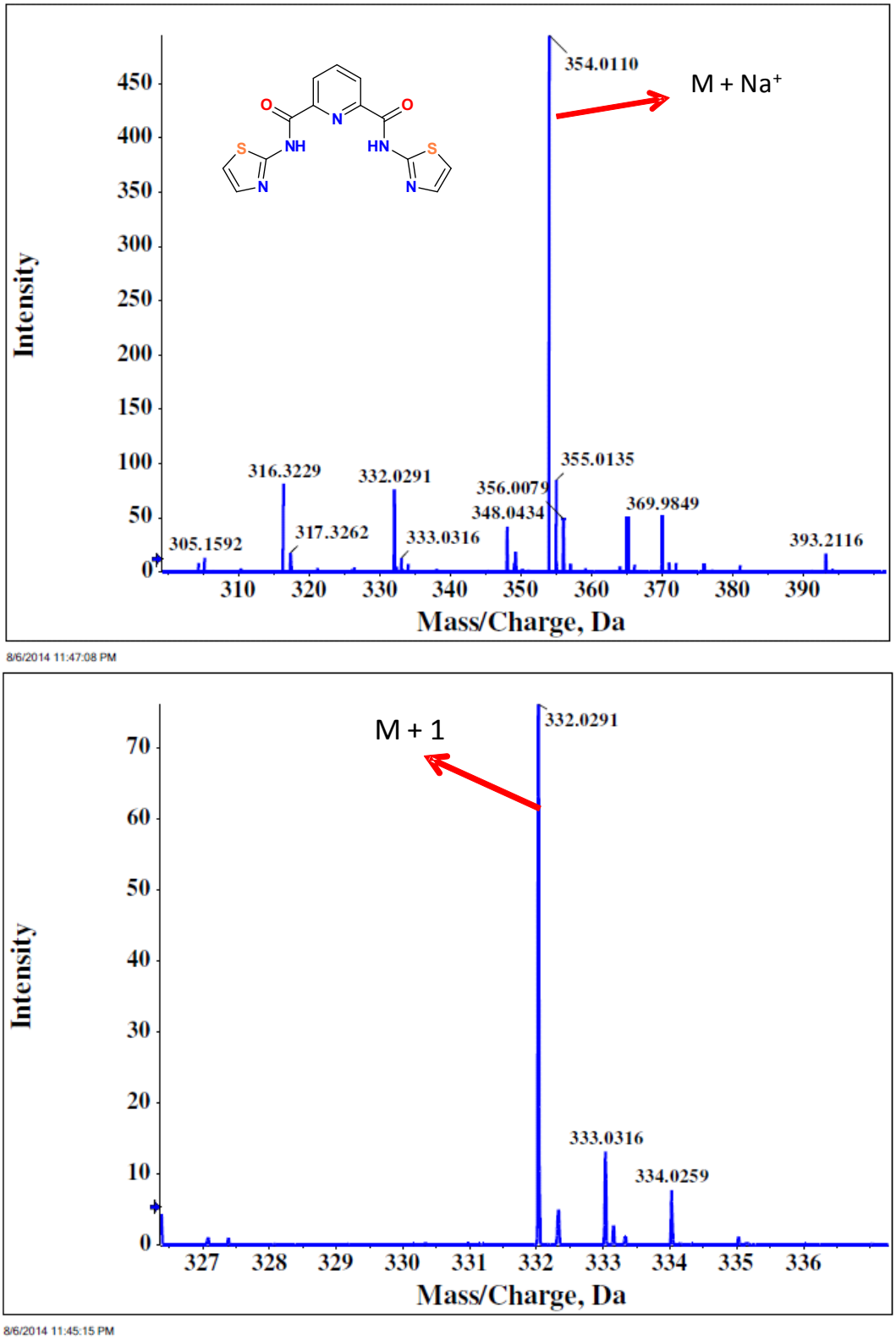

Figure S7. ESI$^+$ mass spectrum of ligand H_2L^1 recorded in $CHCl_3$. Bottom panel displays a zoomed portion out of top panel.

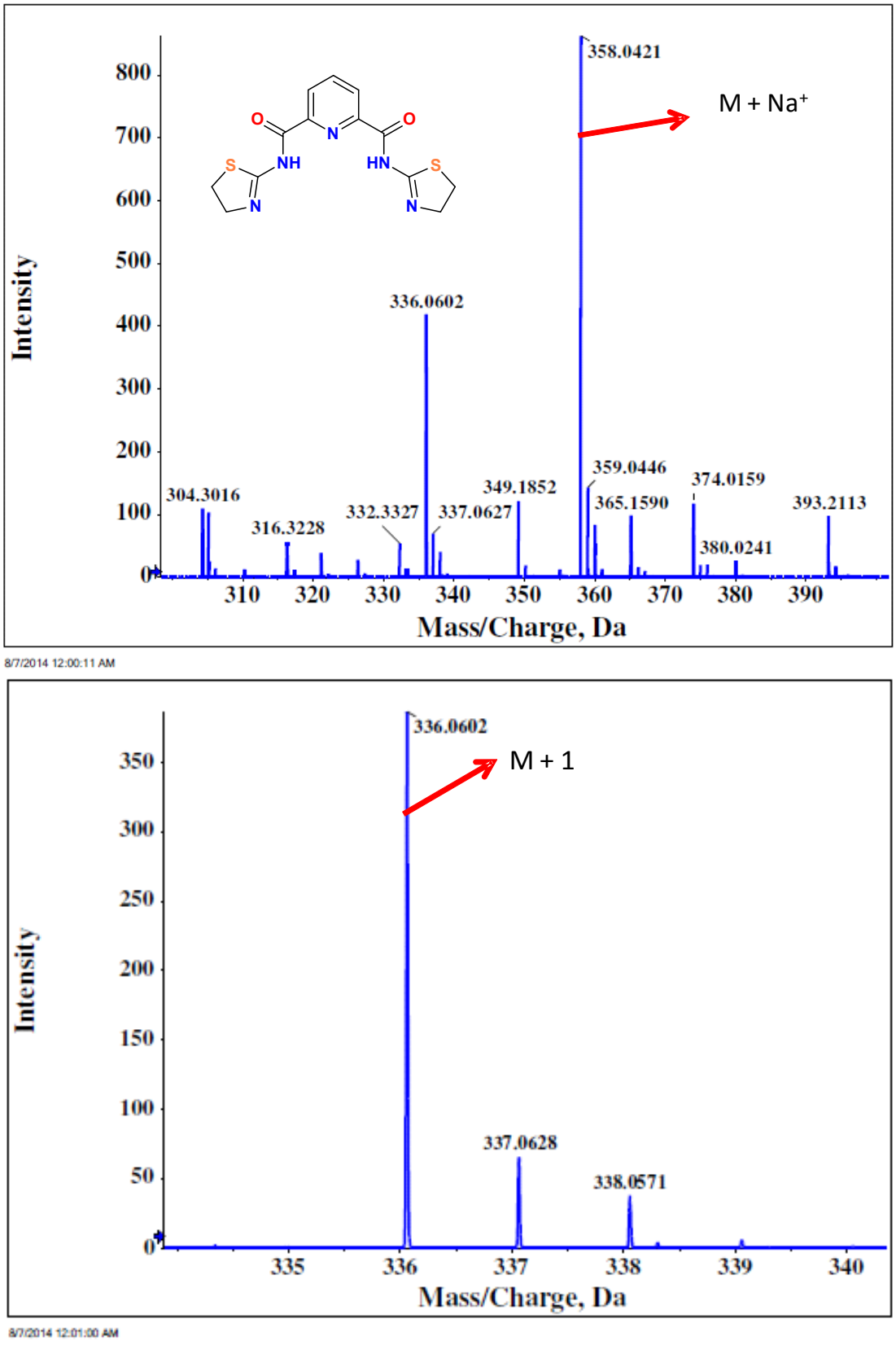

Figure S8. ESI^+ mass spectrum of ligand H_2L^2 recorded in $CHCl_3$. Bottom panel displays a zoomed portion out of top panel.

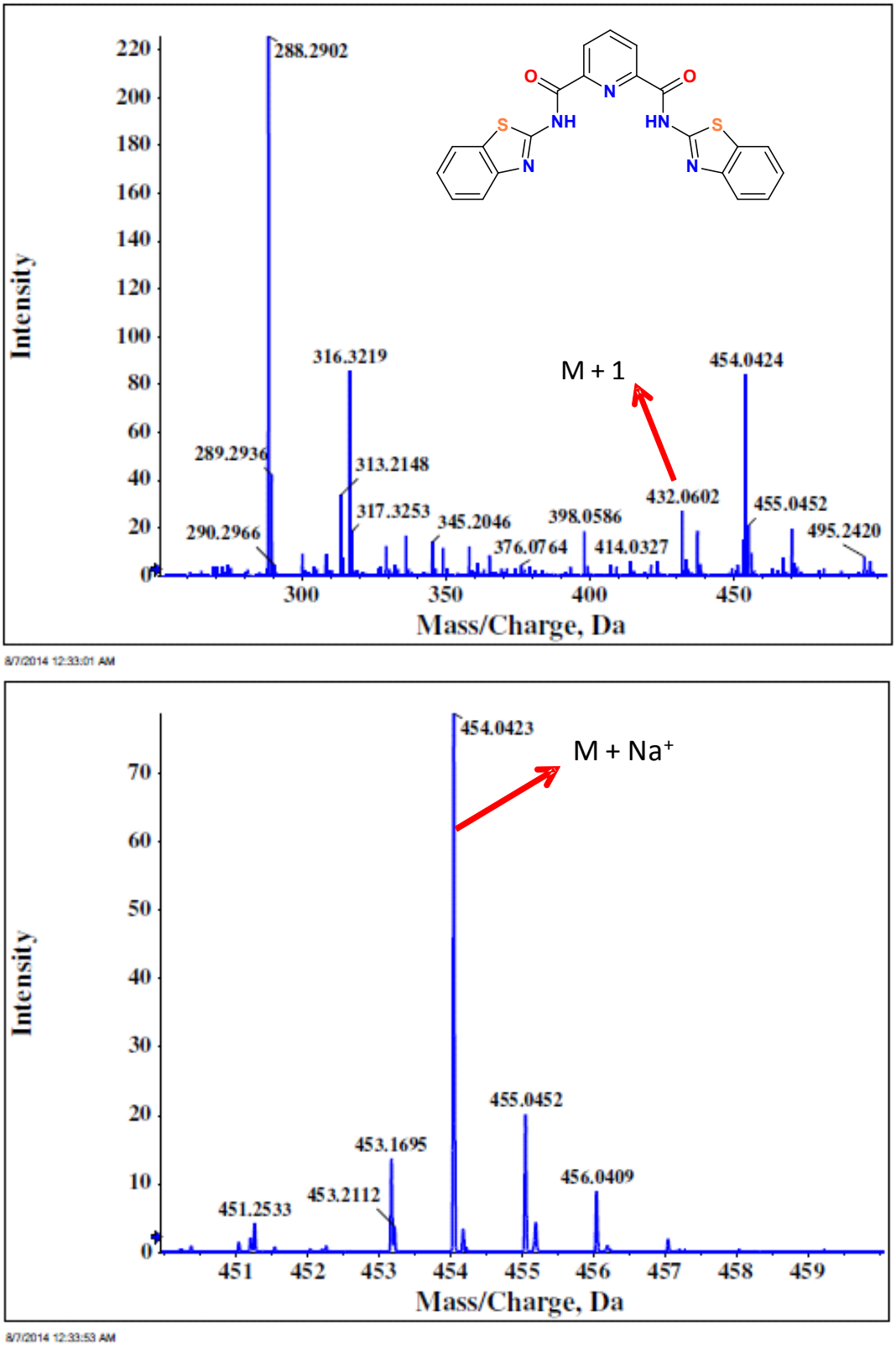

Figure S9. ESI$^+$ mass spectrum of ligand H_2L^3 recorded in THF. Bottom panel displays a zoomed portion out of top panel.

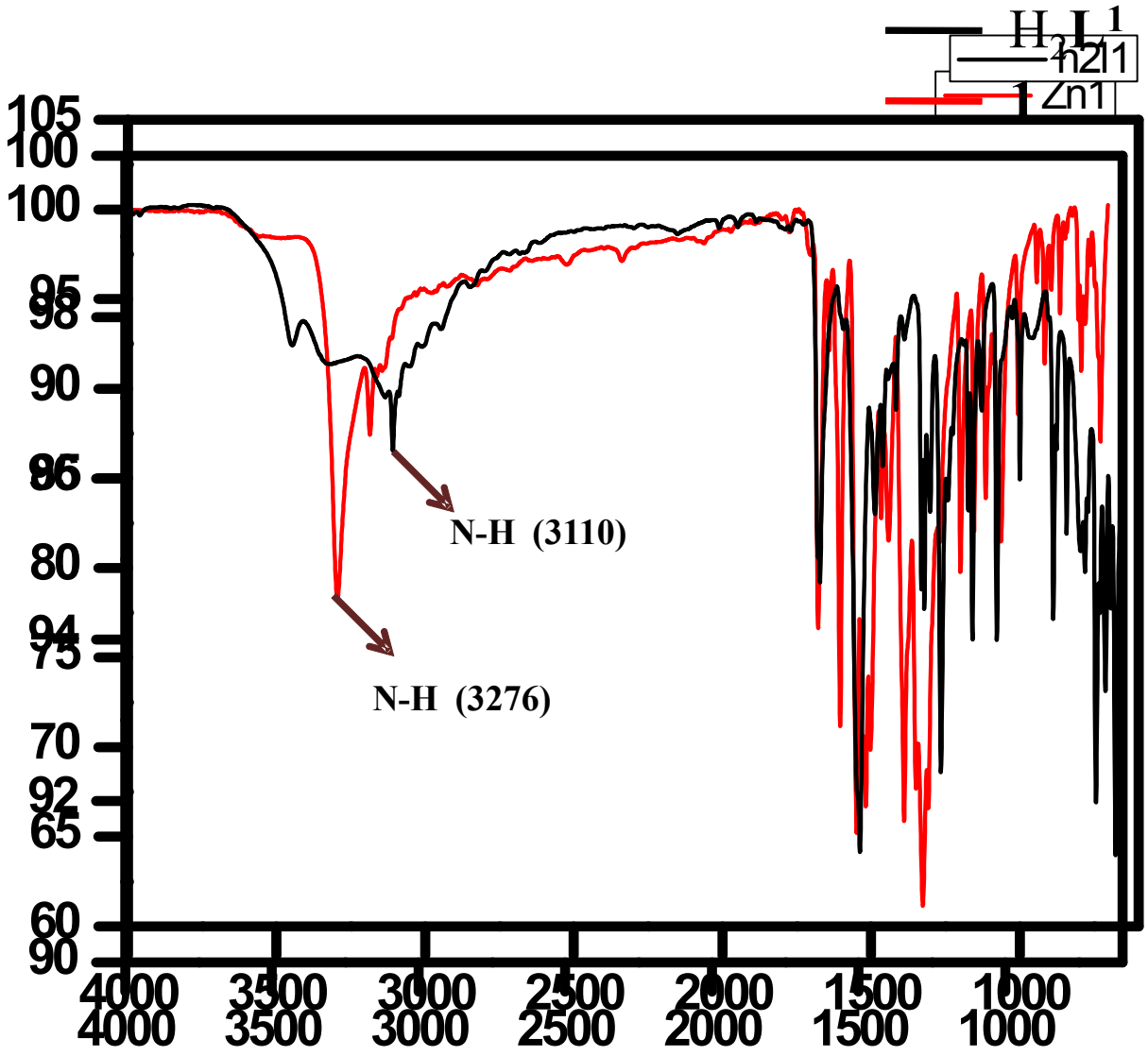

Figure S10. Comparative FTIR spectra of complex **1** (red) and ligand H_2L^1 (black) showing shift of N–H stretches.

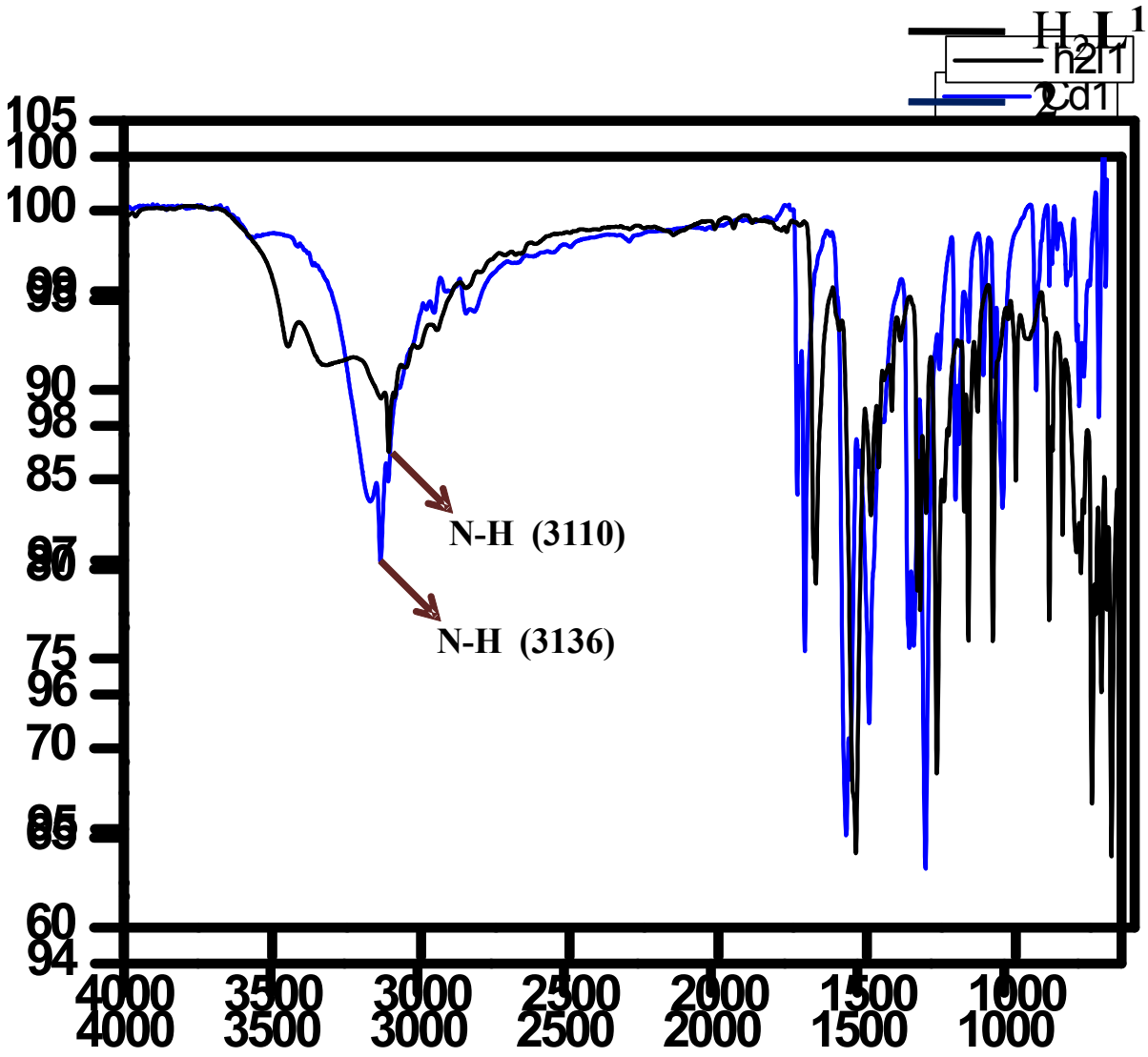

Figure S11. Comparative FTIR spectra of complex **2** (blue) and ligand H_2L^1 (black) showing shift of N–H stretches.

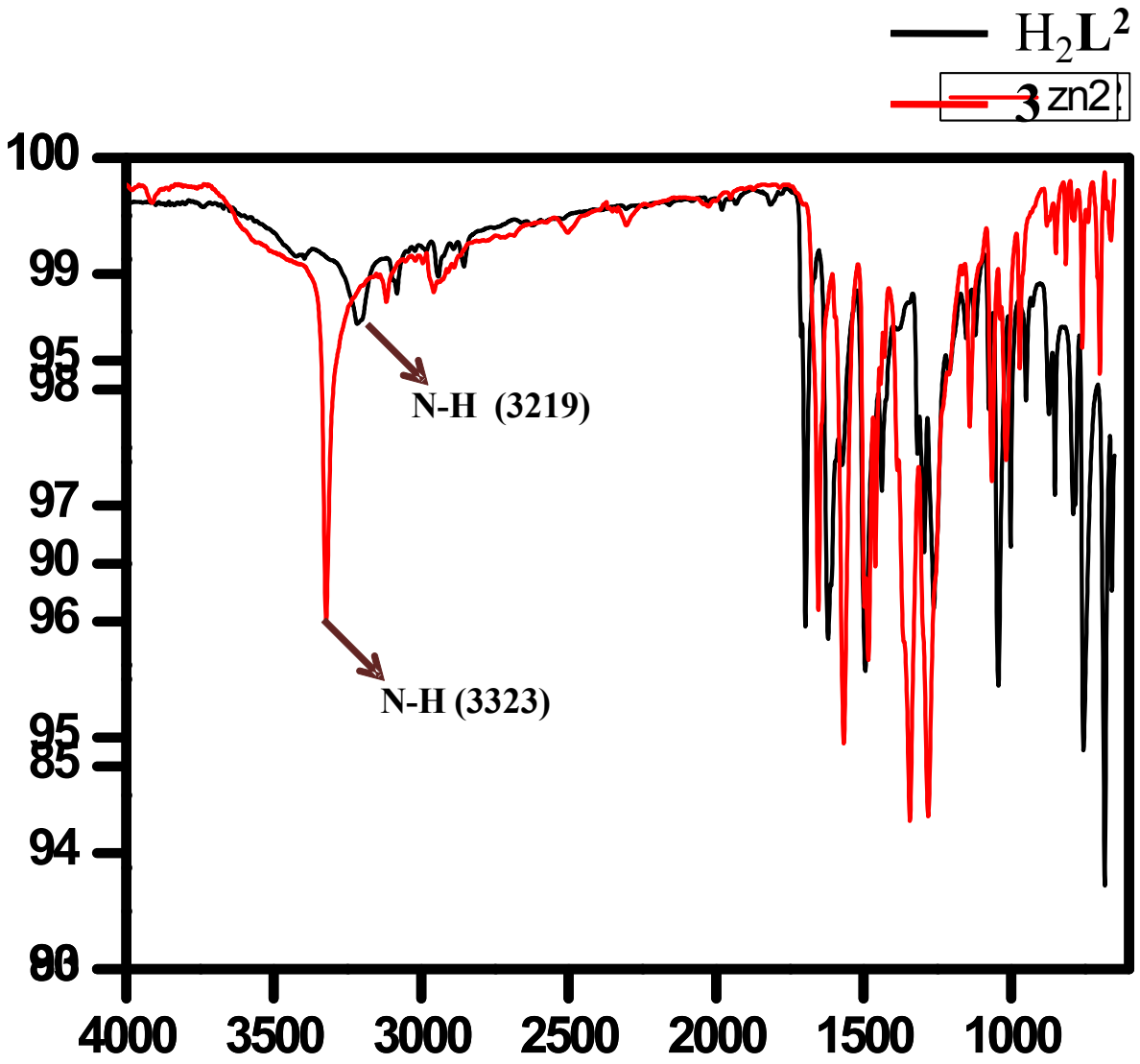

Figure S12. Comparative FTIR spectra of complex **3** (red) and ligand H_2L^2 (black) showing shift of N–H stretches.

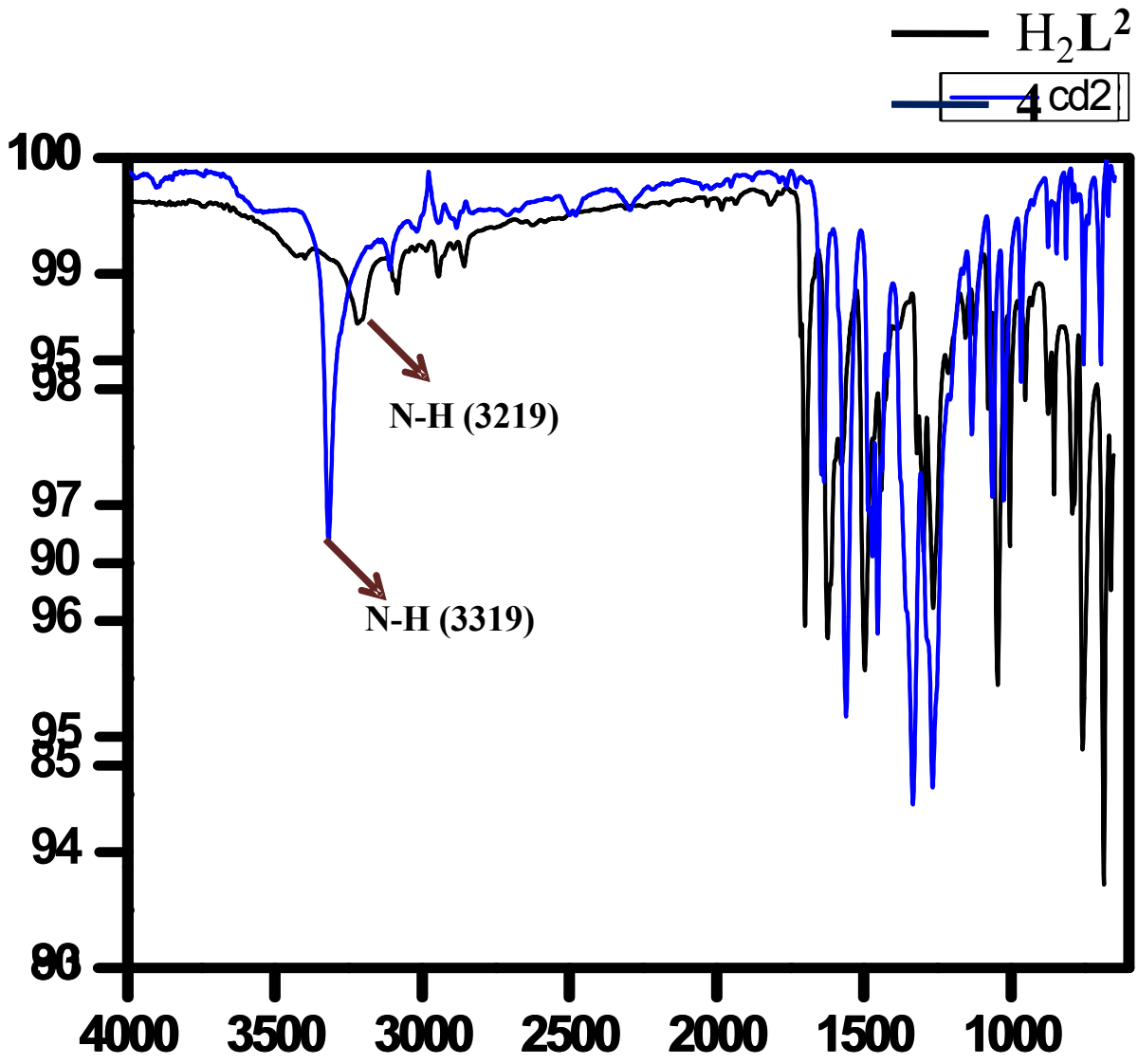

Figure S13. Comparative FTIR spectra of complex **4** (blue) and ligand H_2L^2 (black) showing shift of N–H stretches.

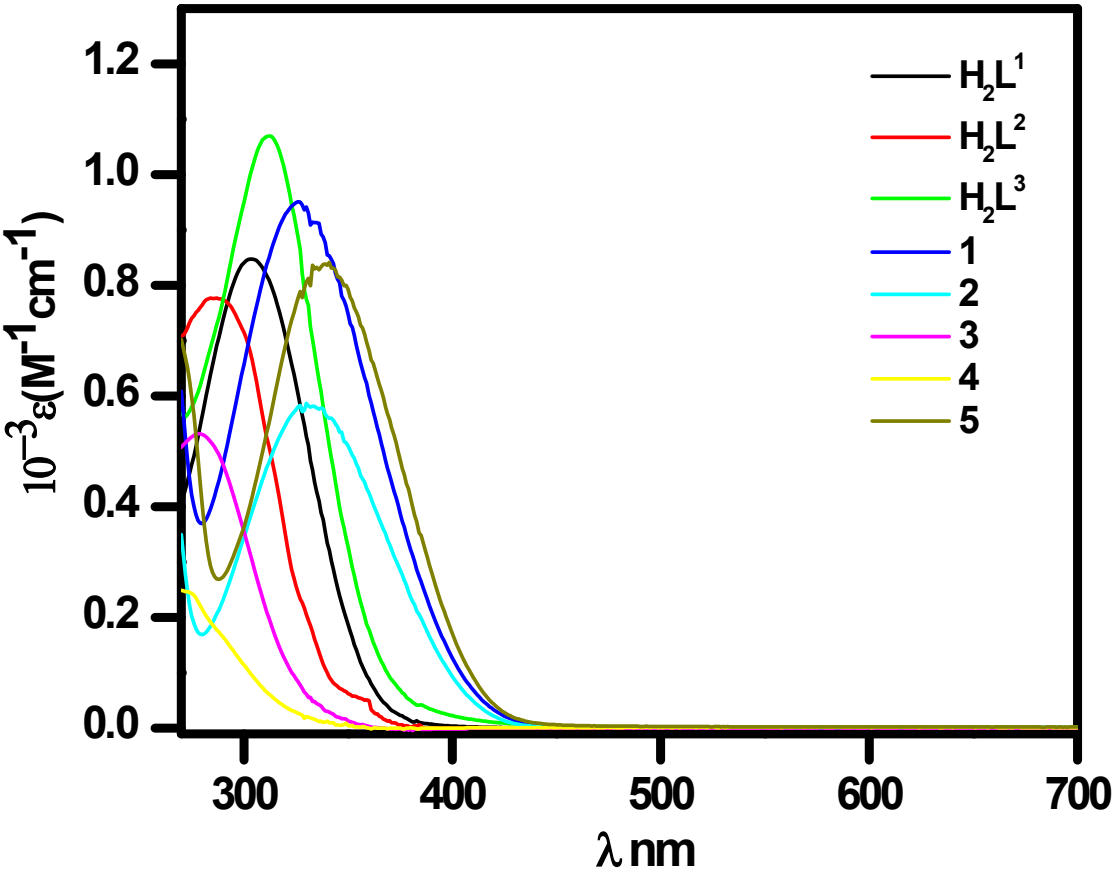

Figure S14. Absorption spectra of ligands H_2L^1, H_2L^2 and H_2L^3 and complexes **1-5** in DMF.

Figure S15. ^{1}H NMR spectrum of complex **1** in d_6-DMSO. * Represents the residual solvent and/or adventitious water.

Figure S16. ^{1}H NMR spectrum of complex **2** in d_6-DMSO. * Represents the residual solvent and/or adventitious water.

Figure S17. ^{1}H NMR spectrum of complex **3** in d_6-DMSO. * Represents the residual solvent and/or adventitious water.

Figure S18. ^{1}H NMR spectrum of complex **4** in d_6-DMSO. * Represents the residual solvent and/or adventitious water.

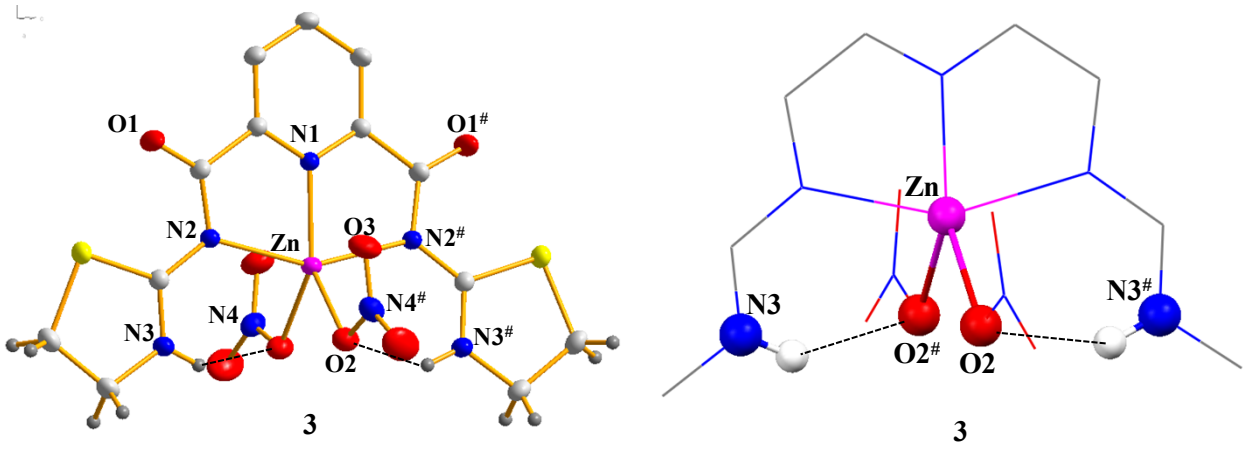

Figure S19. Thermal ellipsoidal representation of complex **3**. Thermal ellipsoids are drawn at 30% probability level whereas only selected hydrogen atoms are shown for clarity. Ringht panel: secondary coordination environment created by the protonated heterocyclic rings around the coordinated nitrate ion in complex **3**.

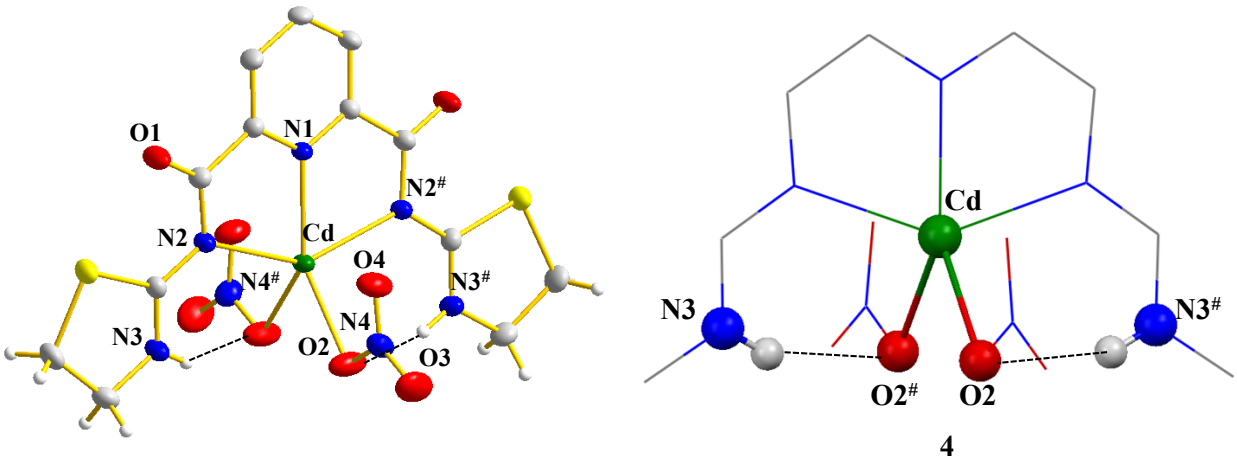

Figure S20. Thermal ellipsoidal representation of complex **4**. Thermal ellipsoids are drawn at 30% probability level whereas only selected hydrogen atoms are shown for clarity. Ringht panel: secondary coordination environment created by the protonated heterocyclic rings around the coordinated nitrate ion in complex **4**.

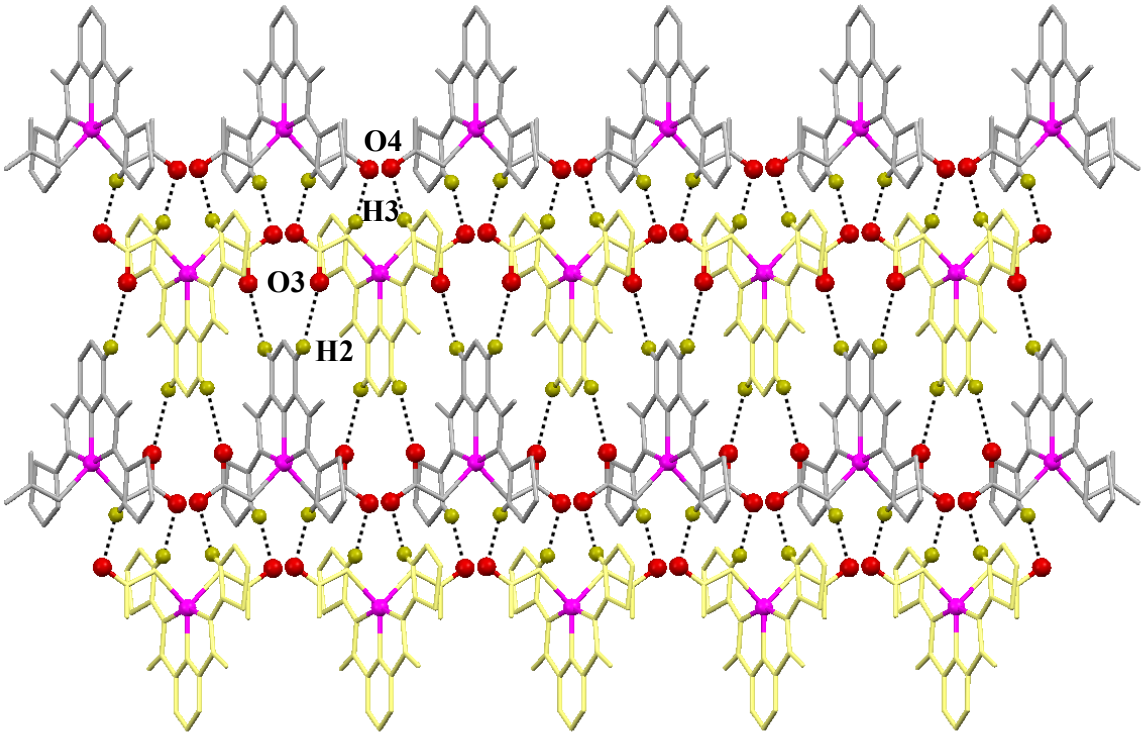

Figure S21. Weak interactions and packing diagram of complex **1** in a view along *a* axis. Selected hydrogen atoms have been shown for clarity.

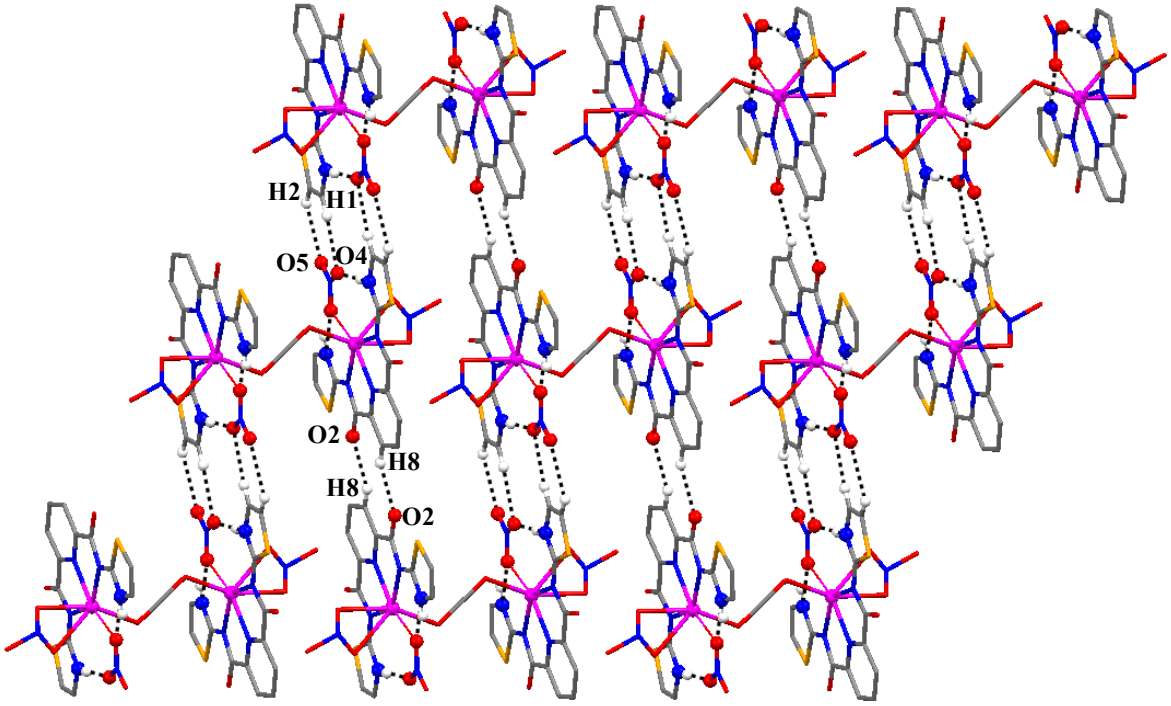

Figure S22. Weak interactions and packing diagram of complex **2** in a view along *b* axis. Selected hydrogen atoms have been shown for clarity.

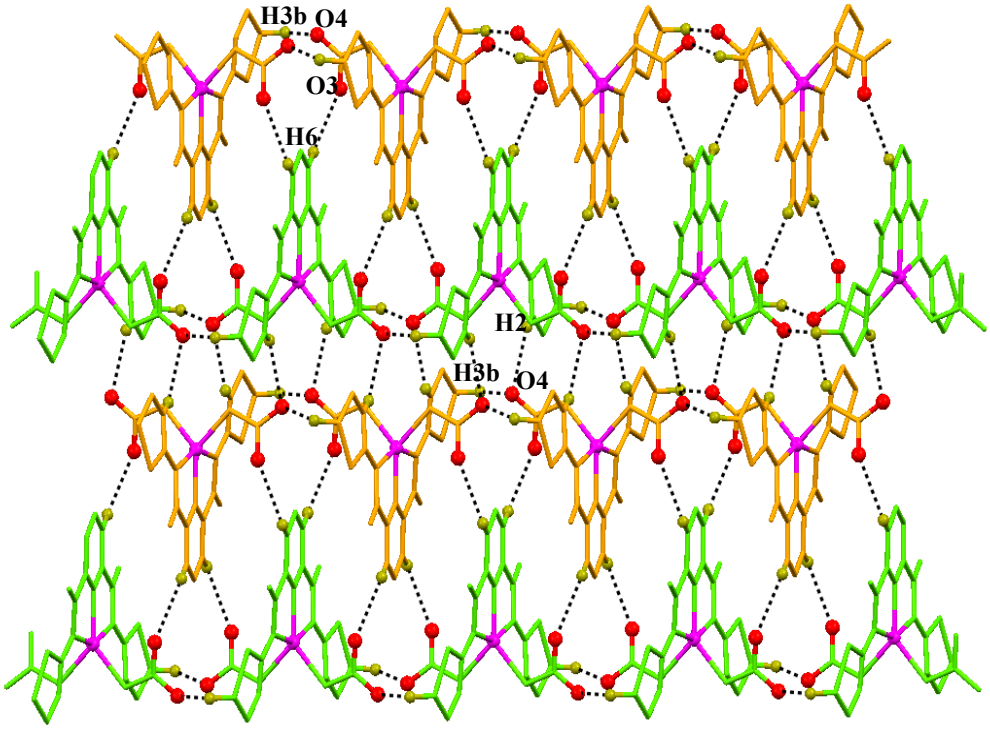

Figure S23. Weak interactions and packing diagram of complex **3** in a view along *a* axis. Selected hydrogen atoms have been shown for clarity.

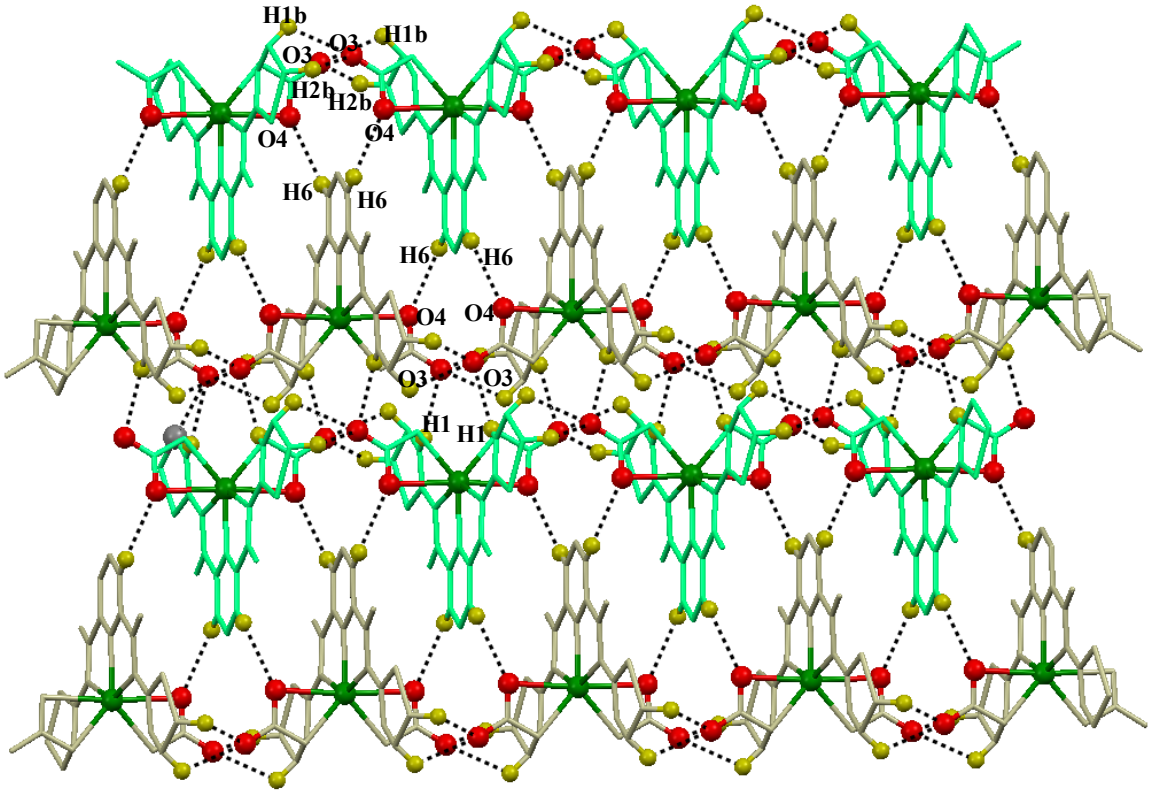

Figure S24. Weak interactions and packing diagram of complex **4** in a view along *a* axis. Selected hydrogen atoms have been shown for clarity.

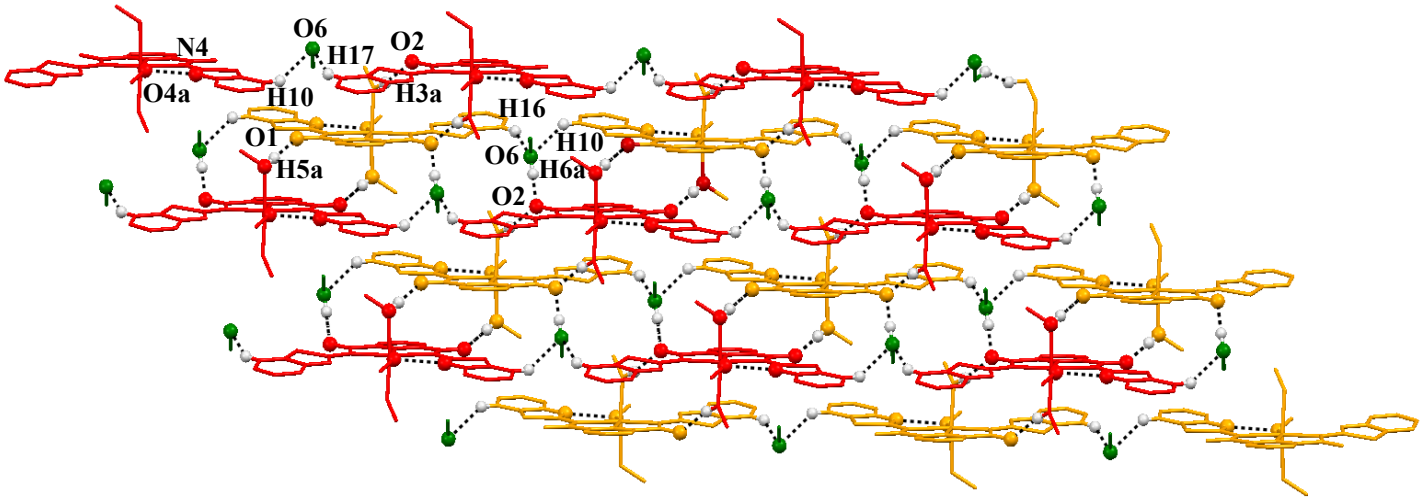

Figure S25. Weak interactions and packing diagram of complex **5** in a view along *b* axis. Selected hydrogen atoms have been shown for clarity.

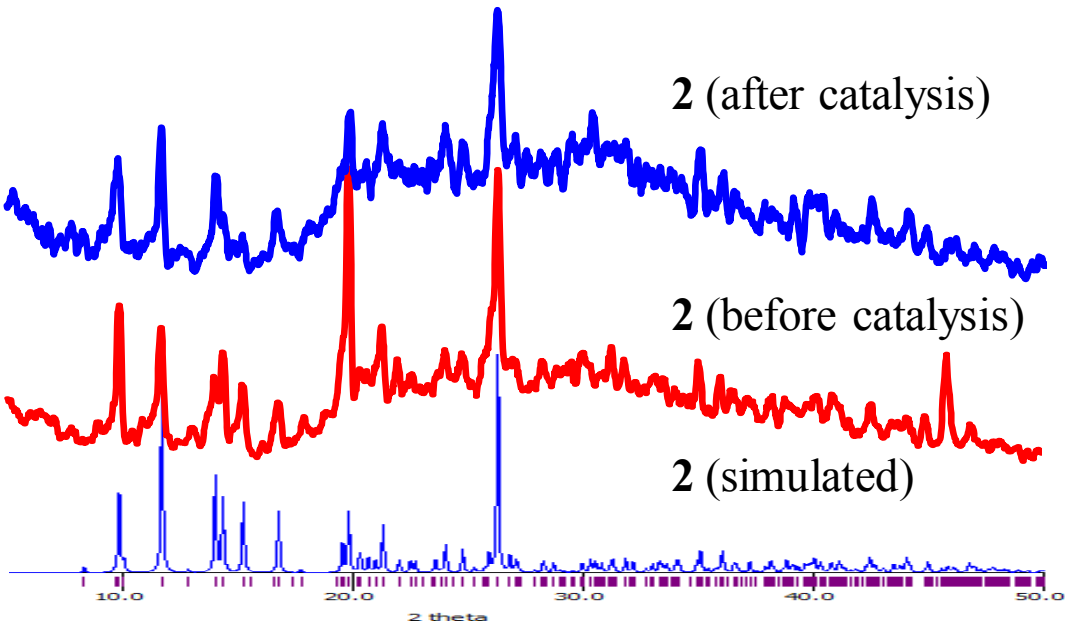

Figure S26. Comparative X-ray powder diffraction patterns of complex **2** with simulated one (bottom) followed by as synthesized (middle) and after (top) ring opening reaction.

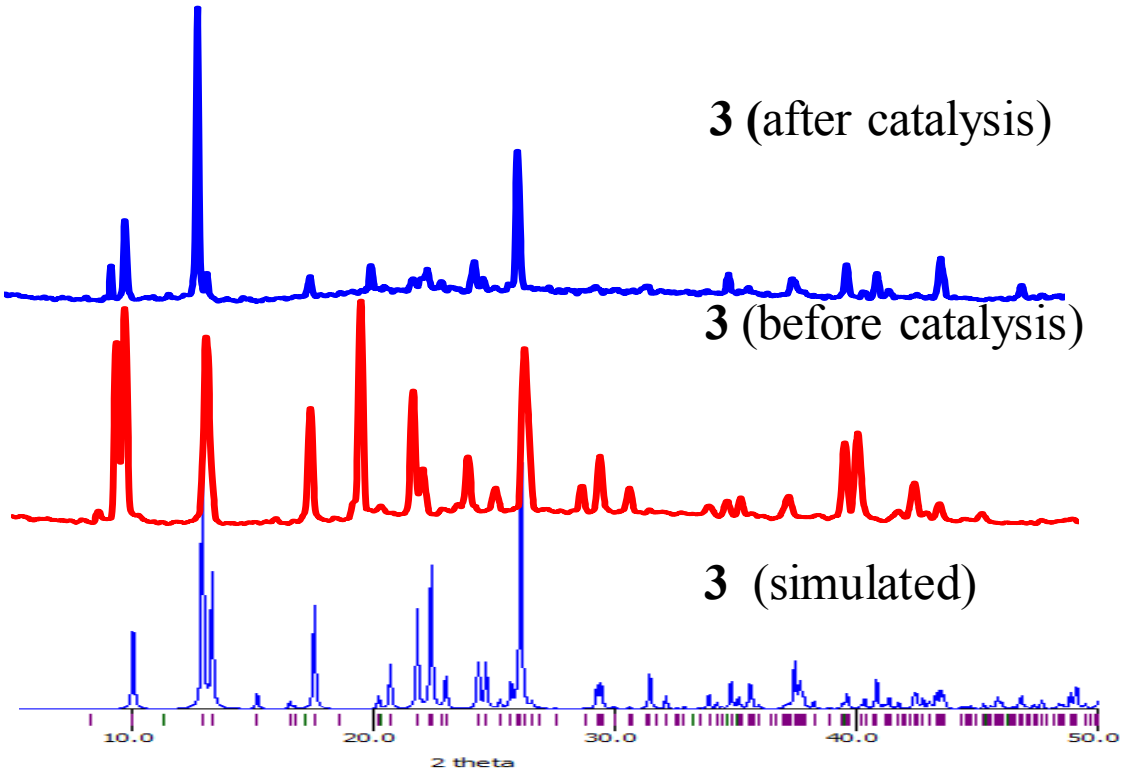

Figure S27. Comparative X-ray powder diffraction patterns of complex **3** with simulated one (bottom) followed by as synthesized (middle) and after (top) ring opening reaction.

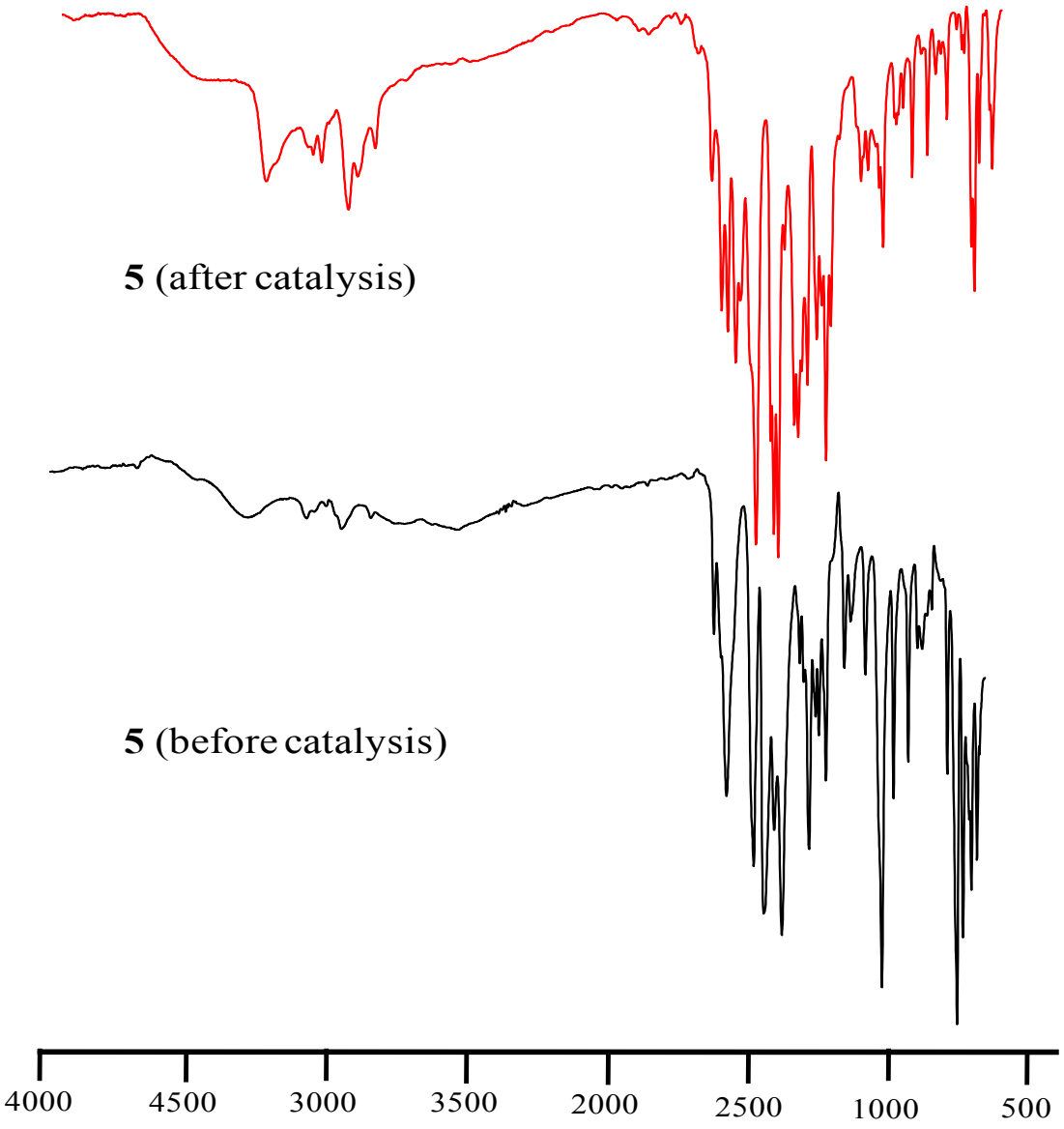

Figure S28. Comparative FTIR spectra of complex **5** before (black) and after epoxidation of styrene (red).

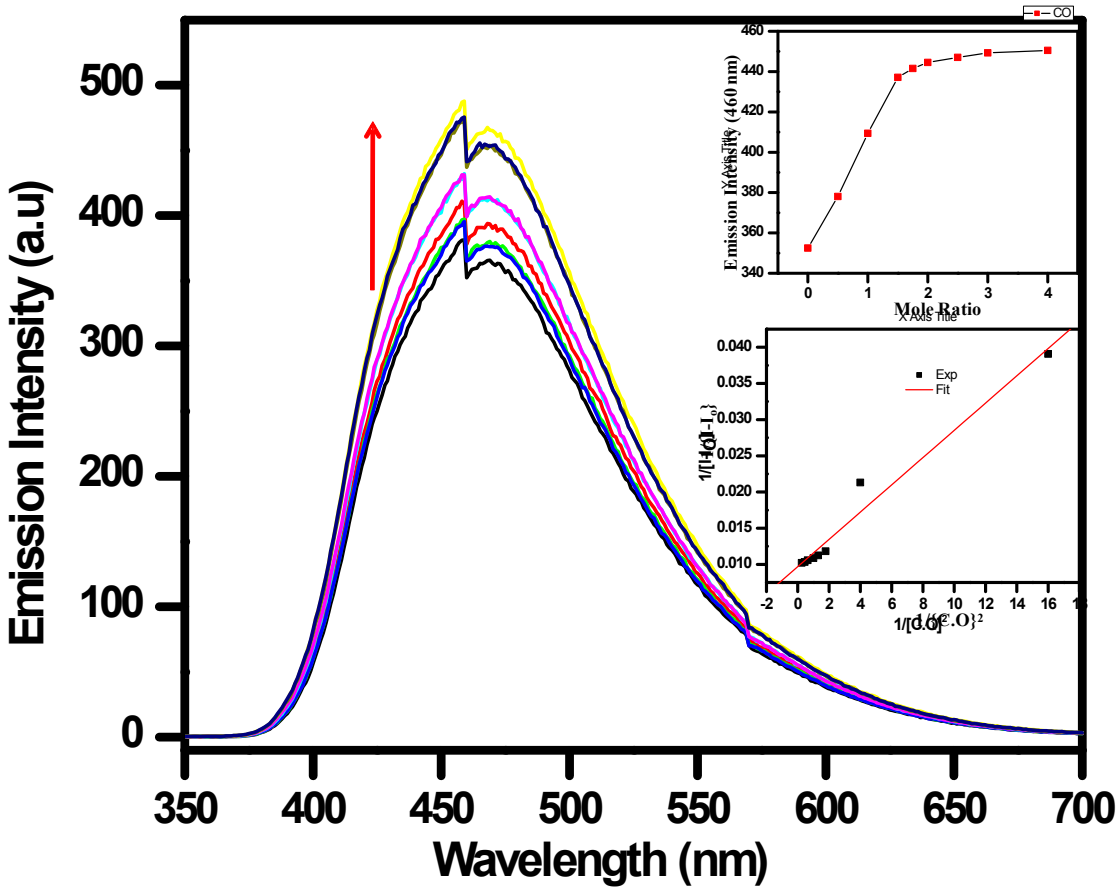

Figure S29. Florescence titration of complex **1** with cyclohexene oxide in DMF-$CHCl_3$ (1:5). Top inset: change in emission intensity as a function of moles of cyclohexene oxide. Bottom inset: Linear regression fitting curve for 1:2 binding between complex **1** and cyclohexene oxide.

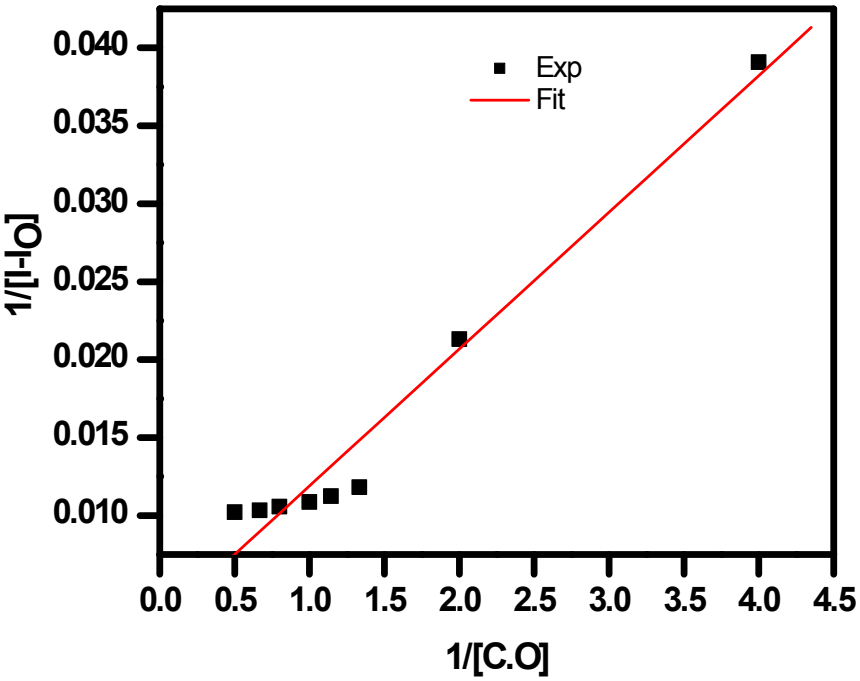

Figure S30. Benesi-Hildebrand plot of complex **1** assuming 1:1 stoichiometry for association between complex **1** and cyclohexene oxide.

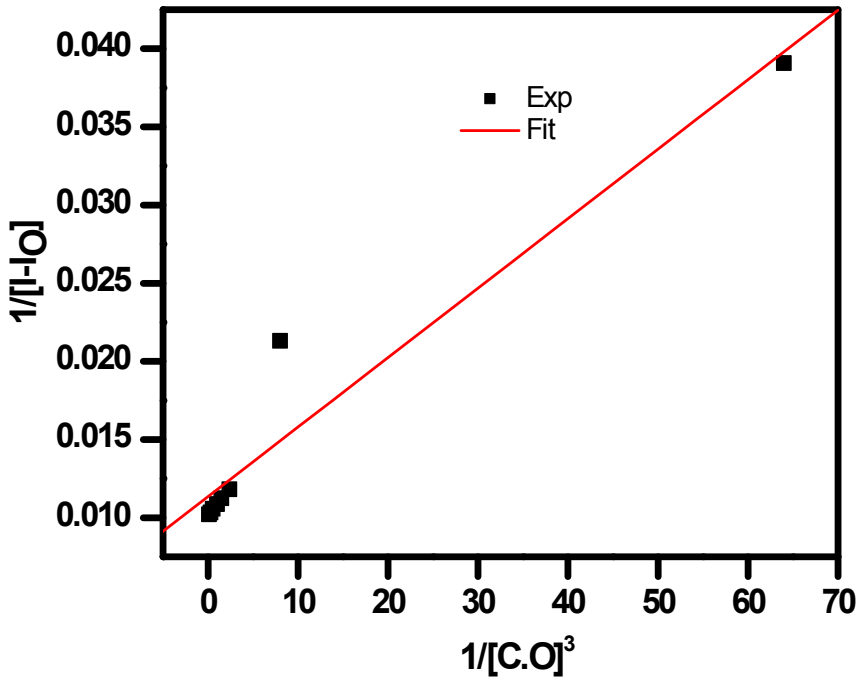

Figure S31. Benesi-Hildebrand plot of complex **1** assuming 1:3 stoichiometry for association between complex **1** and cyclohexene oxide.

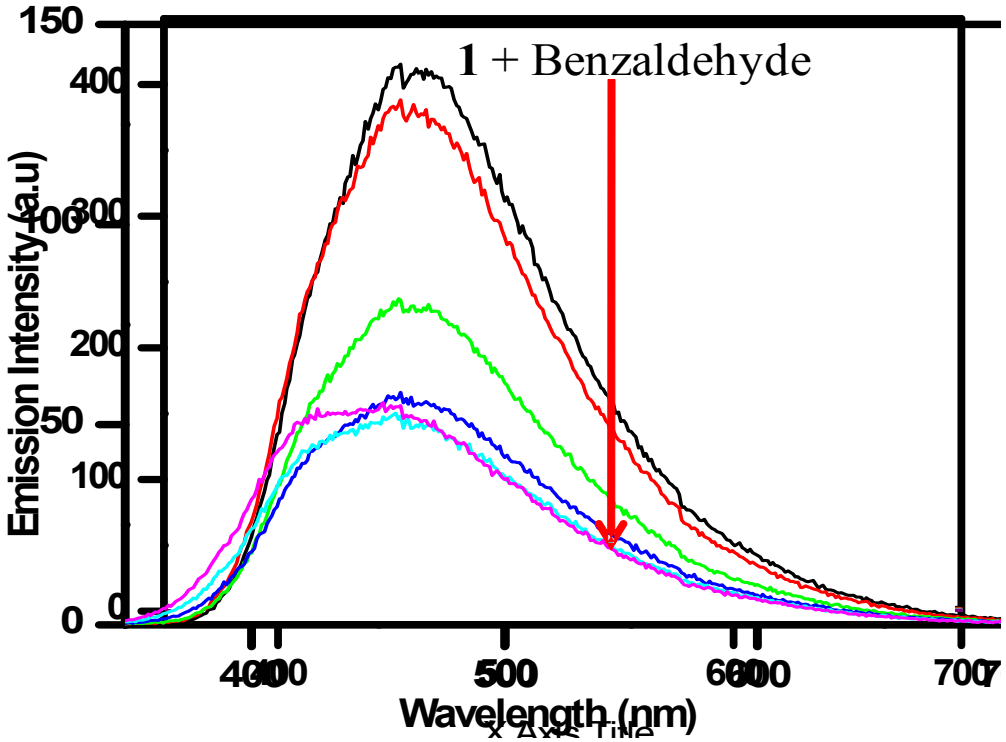

Figure S32. Change in emission intensity of complex **1** (1 mM) on addition of benzaldehyde in $CHCl_3$/DMF (5:1). λ_{ex} = 320 nm.

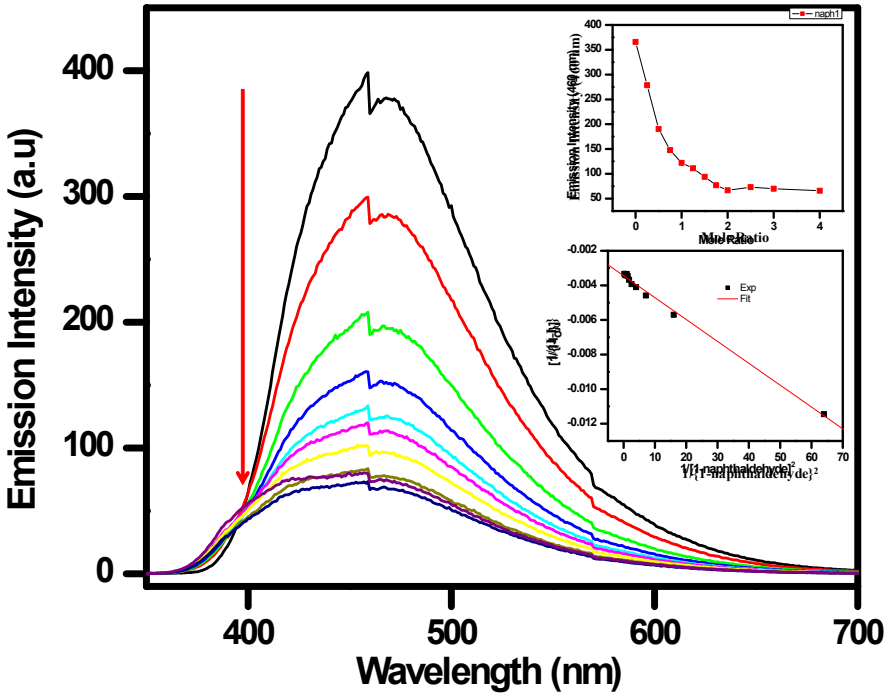

Figure S33. Florescence titration of complex **1** with 1-naphthaldehyde in DMF-$CHCl_3$ (1:5). Top inset: change in emission intensity as a function of moles of 1-naphthaldehyde. Bottom inset: Linear regression fitting curve for 1:2 binding between complex **1** and 1-naphthaldehyde.

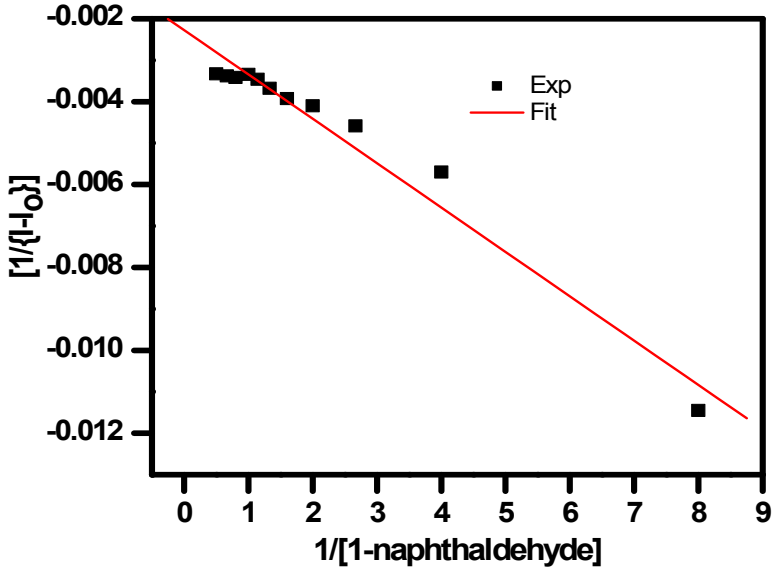

Figure S34. Benesi-Hildebrand plot of complex **1** assuming 1:1 stoichiometry for association between complex **1** and 1-naphthaldehyde.

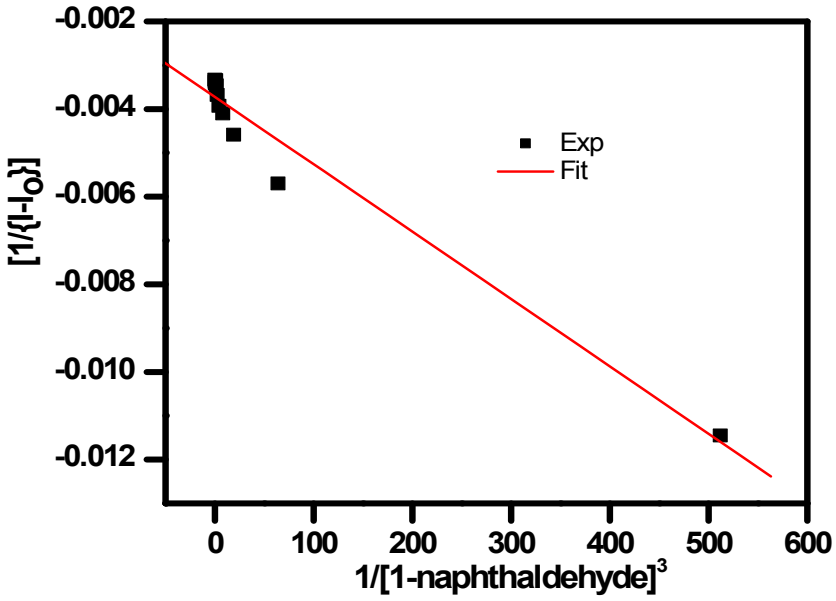

Figure S35. Benesi-Hildebrand plot of complex **1** assuming 1:3 stoichiometry for association between complex **1** and 1-naphthaldehyde.

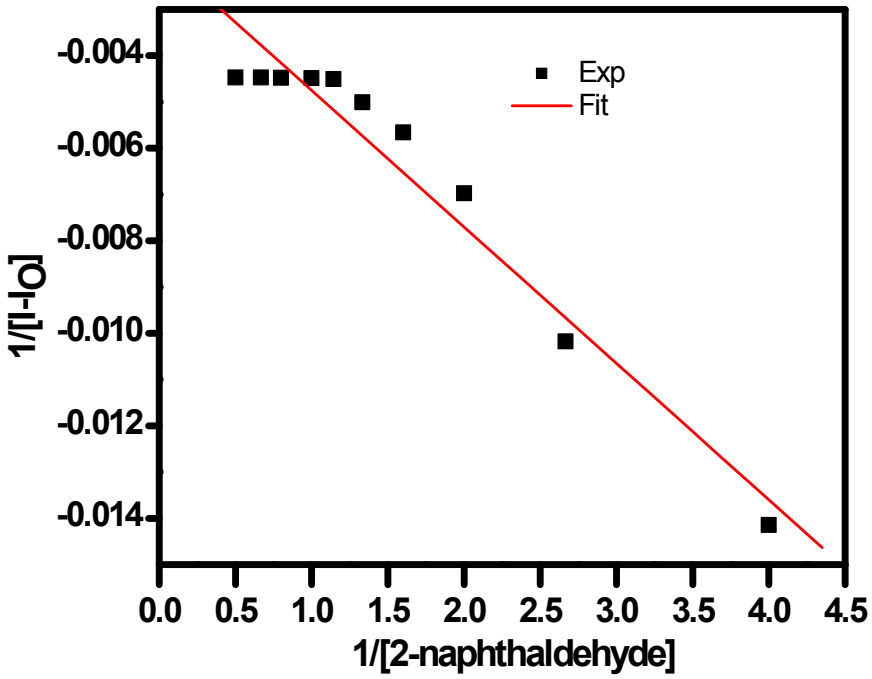

Figure S36. Benesi-Hildebrand plot of complex **1** assuming 1:1 stoichiometry for association between complex **1** and 2-naphthaldehyde.

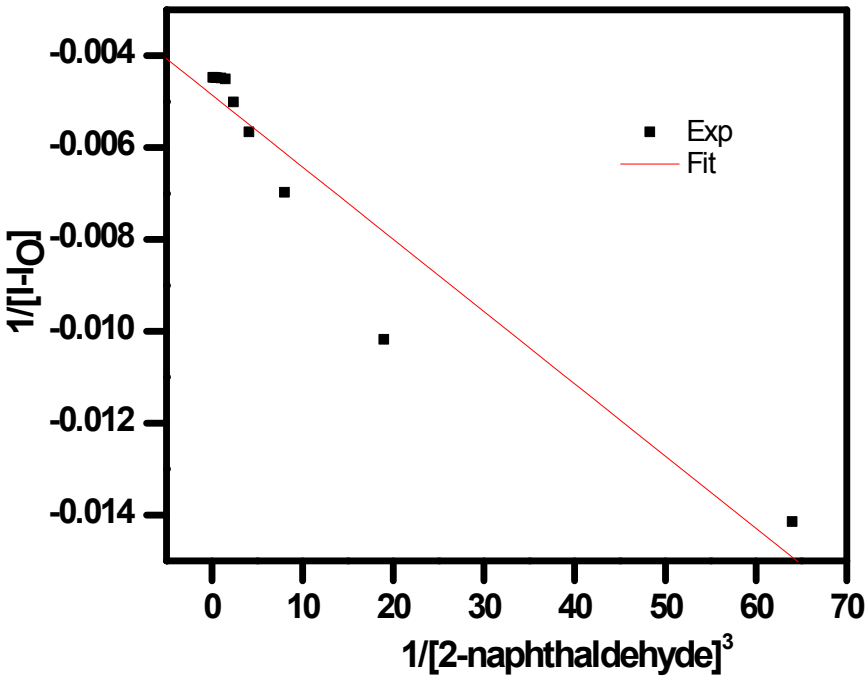

Figure S37. Benesi-Hildebrand plot of complex **1** assuming 1:3 stoichiometry for association between complex **1** and 2-naphthaldehyde.

Table S1. Selected bond lengths (Å) and bond angles (°) for complexes **1**, **3**, **4** and **5**.

Bond	**1**[a]	**3**[b]	**4**[c]	Bond	**5**
M-N1	2.034(1)	2.038(2)	2.255(4)	Mn-N1	2.2234(2)
M-N2	2.173(1)	2.206(2)	2.378(3)	Mn-N2	2.3013(2)
M-O2	2.027(1)	2.043(2)	2.276(3)	Mn-N3	2.2701(2)
M-O4	-------	-------	2.546(3)	Mn-O3	2.1799(2)
O2$^{\#}$-M-O2	88.64(5)	84.34(9)	81.54(7)	Mn-O5	2.2052(2)
O2$^{\#}$-M-N1	135.68(3)	137.83(4)	139.46(8)	O3-Mn-N1	96.12(6)
O2$^{\#}$-M-N2	100.54(4)	97.37(6)	105.76(12)	O5-Mn-N1	90.45(6)
O2-M-N2	98.09(4)	102.84(6)	102.11(12)	O3-Mn-N3	87.52(6)
N1-M-N2$^{\#}$	76.93(3)	76.32(4)	71.54(7)	O5-Mn-N3	91.31(6)
N2-M-N2$^{\#}$	153.86(5)	152.64(8)	143.08(14)	N1-Mn-N3	71.16(7)
-----	-----	-----	-----	O3-Mn-N2	94.09(6)
-----	-----	-----	-----	O5-Mn-N2	91.30(6)
-----	-----	-----	-----	N1-Mn-N2	71.41(6)

[a] # = –x+2, y, -z5/2; [b] # = –x, y, -z+1/2; [c] # = –x, y, -z+3/2.

Table S2. Selected bond lengths (Å) and bond angles (°) for complex **2**.

Bond		**2**	
N2-Cd	2.366(6)	O9-Cd-N2	77.6(4)
N3-Cd	2.262(5)	N3-Cd-N4	70.83(2)
N4-Cd	2.405(5)	O3-Cd-N4	86.5(2)
O6-Cd	2.535(13)	O9-Cd-N4	118.5(3)
O7-Cd	2.488(13)	N2-Cd-N4	141.91(2)
O3-Cd	2.262(7)	O9-Cd-O7	158.2(4)
O9-Cd	2.474(12)	O9-Cd-N2	77.6(4)
N3-Cd-O3	157.1(2)	O6-Cd-O7	48.9(4)
N3-Cd-O9	110.4(4)	N2-Cd-O7	88.5(3)
O3-Cd-O9	77.8(4)	N4-Cd-O7	82.8(3)
N3-Cd-N2	71.25(2)	N3-Cd-O6	122.0(3)
O3-Cd-N2	131.67(3)	O3-Cd-O6	70.7(3)
N3-Cd-O7	80.1(3)	O9-Cd-O6	111.4(5)
O3-Cd-O7	100.0(3)	N2-Cd-O6	80.6(3)
N4-Cd-O6	118.5(3)	----------	----------

Table S3. H-bonding parameters for complex **1**.

D–H···A	d(H···A) (Å)	d(D···A) (Å)	∠(DHA) (°)
N3–H3… O4 (i)	2.231(21)	2.869(2)	139.02(1.93)
C2–H2…O3 (ii)	2.669(1)	3.177(2)	115.08(8)

(i)-x+2, -y+1, -z+2 (ii) –x+2, -y, -z+2

Table S4. H-bonding parameters for complex **2**.

D–H···A	d(H···A) (Å)	d(D···A) (Å)	∠(DHA) (°)
C8–H8… O2 (i)	2.575(6)	2.831(9)	96.83(0.45)
C2–H2…O4 (ii)	2.621(9)	3.223(12)	122.96(0.59)
C1–H1…O5 (ii)	2.477(2)	3.378(19)	163.09(0.68)
N1–H1`… O5 (i)	1.806(3)	2.726(23)	173.42(0.74)
N5–H5`… O3 (i)	1.915(7)	2.747(10)	154.83(0.54)

(i) x, y, z (ii) –x+1, -y+1, -z

Table S5. H-bonding parameters for complex **3**.

D–H···A	d(H···A) (Å)	d(D···A) (Å)	∠(DHA) (°)
C3–H3b… O4 (i)	2.709(3)	3.255(4)	116.17(0.15)
C2–H2…O4 (i)	2.641(3)	3.130(4)	94.56(0.13)
C6–H6…O3 (ii)	2.583(2)	3.133(4)	118.33(0.13)

(i) x, -y, +z+1/2 (ii) x, -y+1, +z+1/2.

Table S6. H-bonding parameters for complex **4**.

D–H···A	d(H···A) (Å)	d(D···A) (Å)	∠(DHA) (°)
C1–H1b… O3 (i)	2.996(4)	3.136(5)	90.97(0.25)
N3–H1… O3 (i)	2.432(3)	2.995(5)	125.24(2.75)
C2–H2b…O3 (ii)	2.714(4)	3.289(7)	118.48(0.28)
C6–H6…O4 (iii)	2.587(3)	3.163(5)	120.55(0.23)

(i) -x+1, -y, -z+2 (ii) –x+1, +y, -z+1/2+2 (iii) x, -y+1, +z-1/2

Table S7. H-bonding parameters for complex **5.**

D–H···A	d(H···A) (Å)	d(D···A) (Å)	∠(DHA) (°)
O4a–H4… N4 (i)	1.876(1)	2.653(3)	155.60(5.01)
C10-H10…O6(i)	2.578(2)	3.387(3)	145.69(0.16)
C17-H17…O6(ii)	2.623(2)	3.443(3)	147.49(0.15)
O3-H3a…O2(iii)	1.937(3)	2.705(2)	168.24(2.94)
O5-H5a…O1(iv)	1.892(3)	2.682(2)	177.77(2.99)
O6-H6a…O2(iv)	1.856(4)	2.798(2)	171.55(3.55)

(i) x, y, z (ii) x+1, +y, +z-1 (iii) -x+1, -y, -z (iv) -x, -y, -z

Table S8. Crystallographic data collection and structural refinement parameters for complexes **1-5**.

	1	**2**	**3**	**4**	**5**
Empirical formula	$C_{13}H_9ZnN_7O_8S_2$	$C_{27}H_{21}Cd_2N_{13}O_{14}S_4$	$C_{13}H_{13}ZnN_7O_8S_2$	$C_{13}H_{13}CdN_7O_8S_2$	$C_{25}H_{28}MnN_5O_6S_2$
formula mass	522.82	1101.58	524.83	571.82	613.58
T [K]	293(2)	293(2)	293(2)	293(2)	293(2)
Crystal system	Monoclinic	Triclinic	Monoclinic	Monoclinic	Monoclinic
Space group	*C*2/c	*P*-1	*C*2/c	*C*2/c	*P*21/c
a [Å]	18.328(16)	8.983(3)	18.227(7)	18.417(4)	12.7166(4)
b [Å]	13.160(11)	9.998(5)	13.241(5)	12.981(5)	22.4097(8)
c [Å]	7.619(7)	11.870(4)	8.076(3)	8.292(4)	9.7068(3)
α [°]	90	114.861(4)	90	90	90
β [°]	104.262(4)	98.299(2)	105.998(2)	105.024(3)	100.694(3)
γ [°]	90	95.304(5)	90	90	90
V [Å3]	1781.2(3)	943.1(7)	1873.6(12)	1914.6(13)	2718.15(15)
Z	4	1	4	4	4
d [g cm–3]	1.950	1.940	1.861	1.984	1.499
μ [mm–1]	1.679	1.433	1.597	1.420	0.689
F(000)	1056	543	1064	1136	1272
R(int.)	0.0190	0.0521	0.0385	0.0574	0.0172
Final R indices	R1=0.0215	R1=0.0668	R1=0.0386	R1=0.0367	R1=0.0325
[I>2σ(I)][a,b]	wR2=0.0612	wR2=0.1801	wR2=0.0890	wR2=0.0620	wR2=0.0822
R indices	R1=0.0234	R1=0.0897	R1=0.0663	R1=0.0538	R1=0.0376
(all data)	wR2=0.0625	wR2=0.2019	wR2=0.0994	wR2=0.0697	wR2=0.0847
GOF on F2	0.987	3.297	1.009	1.109	1.029

[a] $R = \sum(\|Fo\| - |Fc|)/\sum|Fo|$, [b] $wR = \{\sum[w(F_o^2 - F_c^2)^2]/\sum[w(F_o^2)^2]\}^{1/2}$

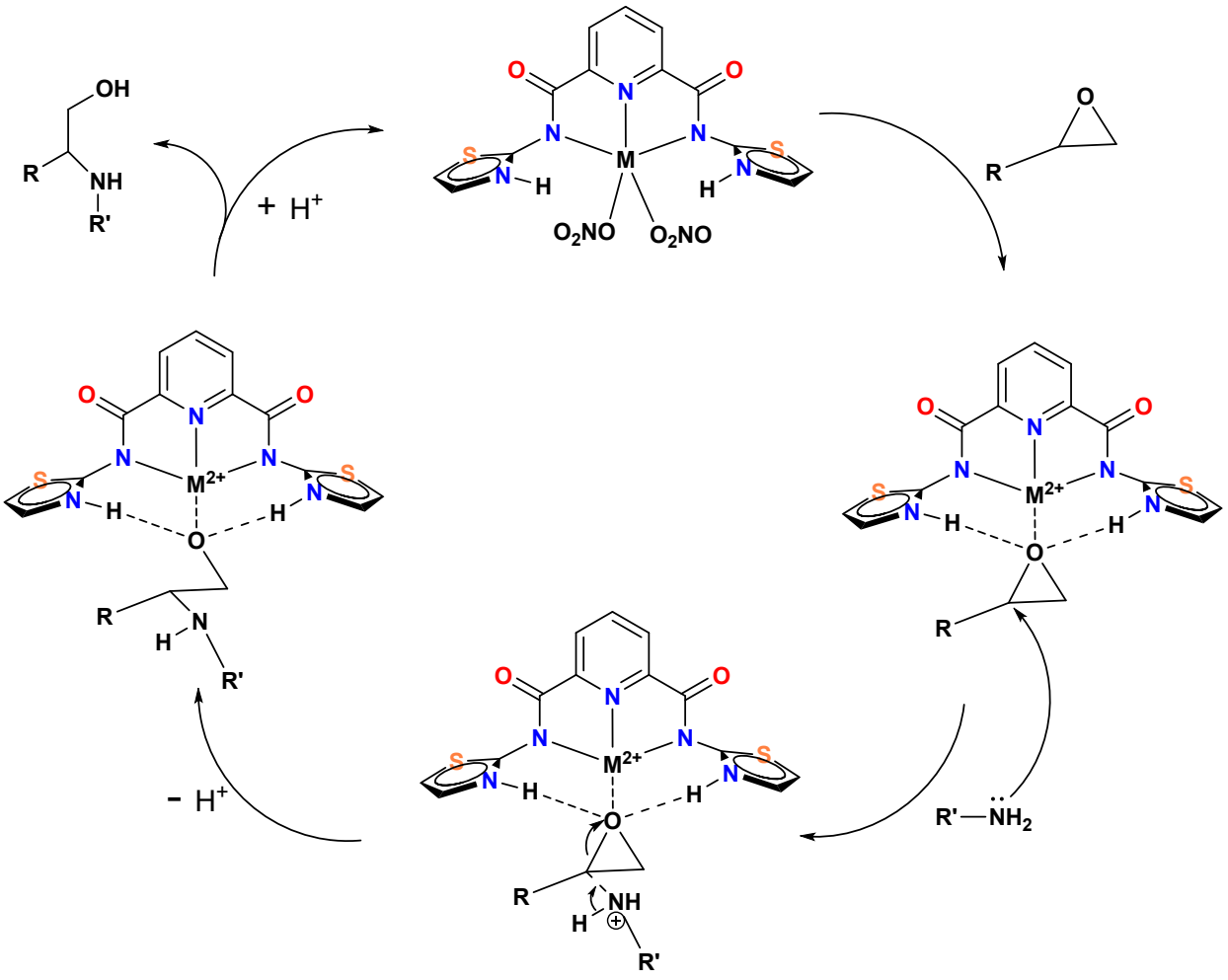

Scheme S1. Proposed mechanism for the ring-opening reaction catalyzed by complex **1** as a represntative example.